Available online at www.sciencedirect.com
ScienceDirect
International Journal of Heat and Mass Transfer 51 (2008) 3924–3931
International Journal of HEAT and MASS TRANSFER
www.elsevier.com/locate/ijhmt

Numerical study of phonon radiative transfer in porous nanostructures

Sheng-Yen Li [a], Hsin-Sen Chu [a], Wei-Mon Yan [b,*]

[a] Department of Mechanical Engineering, National Chiao Tung University, Hsin-Chu 300, Taiwan, ROC
[b] Department of Mechatronic Engineering, Huafan University, Shih-Ting, Taipei 223, Taiwan, ROC

Received 9 June 2007; received in revised form 8 January 2008
Available online 4 March 2008

Abstract

This study analyzes the phonon radiative transfer in two-dimensional porous silicon nanostructures with a phonon transport model based on the Boltzmann transportation equation. We focus on the inter-scattering between pores. The numerical results show that when the aspect ratio is less than 1.22, the scale factor dominates the thermal conductivity, and the thermal conductivity of nanostructures with in-line arrangement pores is determined by the dependent phonon scattering effect. In nanostructures with staggered arrangement pores, the phonons are prevented from transporting through the material. In general, the results show that the larger the pore size, the lower the thermal conductivity of the nanostructure. The results presented in this study provide a useful reference for the development of high-efficiency thermoelectric structures.

1. Introduction

The issue of phonon transportation in semiconductors has received considerable attention over the past decade [1,2]. When the characteristic size of a device is close to the mean free path (MFP) of the phonons, the thermal conductivity of the device material is determined by its weight, size and temperature. Phonon transport is a highly important mechanism of heat transfer in semiconductor nanostructures, and dominates their thermal conductivity properties [3–5].

For nanostructure material, its internal structure highly affects the phonon transport process. Particular attention has been paid to super lattices over the past decade [4–6], which are periodic structures consisting of alternating layers of two semiconductor materials. Due to the existing of surface roughness, the phonons are scattered at the interfaces between adjacent layers when they are transported through the structure, which causes the thermal conductivity of the device to become lower than that of the bulk material. Besides, the mismatch in lattice vibrated properties hampered the phonon transport between heterogonous materials and diffuse mismatch model (DMM) is developed to estimate it [7]. If the device size is comparable to or even smaller than the MFP, the phonons may be transported ballistically, and the interfacial resistance dominates the thermal conductivity. Taking Bi_2Te_3/Sb_2Te_3 as an example, the thermal conductivity of the super lattice is 0.5 W m^{-1} K^{-1}, whereas that of the bulk is 2.0 W m^{-1} K^{-1} at 300 K [8]. Conjugate gradient method is utilized to solve the inverse phonon radiant transport problem in double-layer nanoscale thin film. It is also improved while the thickness of films increases, the temperature jumps at the boundaries and interface become negligible. In other words, interface resistance may play an important role as size effect dominates [9].

One of the most effective methods of reducing the thermal conductivity of a nanostructure material is to increase phonon scattering at the interface. Phonon transport in quantum dot thin films and quantum dot super lattices has been investigated both numerically and experimentally [10–12]. In general, the results showed that the phonons are scattered at the boundaries of the quantum dots, and the larger the radius of the quantum dots, the lower the thermal conductivity of the structure.

* Corresponding author. Tel.: +886 2 26632102; fax: +886 2 26633234.
E-mail address: wmyan@huafan.hfu.edu.tw (W.-M. Yan).

0017-9310/$ - see front matter © 2008 Elsevier Ltd. All rights reserved.
doi:10.1016/j.ijheatmasstransfer.2008.01.004

Nomenclature

A	aspect ratio [$L_W L_H^{-1}$]	m	total number of grids in x direction
a	the number of grids in x direction	n	total number of grids in y direction
b	the number of grids in y direction	q	heat flux [W m^{-2}]
c	specific heat [kJ kg K^{-1}]	T	temperature [K]
I	phonon radiative intensity [W m^{-2} s^{-1} r^{-1}]	T_{avg}	average temperature [K]
I_0	phonon radiative intensity in energy equilibrium [W m^{-2} s^{-1} r^{-1}]	v	phonon group velocity [m s^{-1}]
K	thermal conductivity [W m^{-1} K^{-1}]	w	weights of DOM
$K_{eff.}$	effective thermal conductivity in nano-structure [W m^{-1} K^{-1}]	*Greek symbols*	
L	system size [nm]	θ	polar angle
L_P	pore size [nm]	ϕ	azimuthal angle
		η	dimensionless temperature $(T - T_1)(T_2 - T_1)^{-1}$

Nanowires and super lattice nanowires have similar structures to super lattice [13–16]. The thermal conductivity of super lattice nanowires is lower than that of super lattices as a result of radial phonon transport confinement, and it increases with nanowire radius. Other micro- and nanoscale structures such as porous thin films and nanocomposites also increase phonon scattering, and therefore reduce the thermal conductivity [19,20]. Furthermore, phonon boundary scattering in nanowires leads to a reduced phonon mean free path and reduced thermal conductivity. This suggests that the development of nanostructures provides the possibility of using confinement effects to increase S and σ, while reducing K [21].

The total thermal resistance of a device includes the interfacial thermal resistance between two adjacent layers of different materials, volumetric scattering resistance, and boundary resistance [16]. Through molecular dynamics simulation, boundaries strongly constrain the movement of phonons in thin film, wire, and nanoparticle [17]. Atomistic Green's function method, moreover, is derived to simulate sophisticated atomic structures [18]. In general, the smaller the device size, the higher the probability of the phonons being scattered at the interface or at the boundaries of internal pores or defects.

As mentioned above, the study of the effect of pore geometry and arrangement (i.e. aligned or staggered) on the thermal conductivity of a 2D porous nanostructure is important and is little in the literature. This motivates the present study in which a phonon transport model based on the Boltzmann transportation equation is developed to explore the effects of the pore geometry and arrangement on the thermal conductivity of a 2D porous nanostructure.

2. Analysis

Phonons are quantized waves and the major heat carriers in semiconductor materials [22]. In the past researches, phonon was treated as particle and phonon intensity can be predicted by Boltzmann transport equation (BTE). Applying the relaxation time approximation in steady state, BTE can be simplified as [4]

$$\nabla I = \frac{\frac{1}{4\pi}\int_{4\pi} I \mathrm{d}\Omega - I_0}{\Lambda} \tag{1}$$

where I_0 is the equilibrium phonon intensity; Λ is the phonon mean free path. The term on the right hand side of Eq. (1) represents the average variation in phonon intensity with the phonon–phonon, phonon–boundary, or phonon–defect collisions within the average MFP. In this work, we assume that the phonon velocity and intensity are uniform in the material. By kinetic theory, the phonon mean free path would be

$$\Lambda = 3\frac{K}{cv}. \tag{2}$$

where c is the specific heat; v is the phonon group velocity; K is the thermal conductivity in bulk. The values of these parameters applied in the present simulations of phonon transportation in a porous silicon nanostructure are presented in Table 1.

Because the behavior of phonon and photon are very alike, we assimilate the phonon intensity to photon intensity. On the assumption that the materials are gray bodies, the phonon intensity varies directly with the temperature T in accordance with the following relationship [23]

$$\frac{\mathrm{d}I}{\mathrm{d}T} = \frac{vc}{4\pi}, \tag{3}$$

By the equation above, at temperature T, the mean phonon intensity can be obtained as I_T in the following equation:

Table 1
Material parameters used in the present study [4]

	c (10^6 J/m^3 K)	v (m/s)	Λ (nm)
Silicon	0.93	1804	268

$$\int_0^T \frac{\mathrm{d}I}{\mathrm{d}T}\mathrm{d}T = I_T = \int_0^T \frac{vc}{4\pi}\mathrm{d}T \tag{4}$$

In this work, we adopt the constant thermal boundary condition, which are

$$T = T_{\mathrm{H}} \quad \text{at } x = 0 \tag{5a}$$

$$T = T_{\mathrm{L}} \quad \text{at } x = L \tag{5b}$$

$$\frac{\partial T}{\partial y} = 0 \text{ at } \quad y = 0 \text{ or } y = L \tag{5c}$$

Additionally, it is important to define the ' thermal conductivity while we discuss thermal physical properties in nanoscale structures. Thermal unbalance had been widely discussed in nano-structures; therefore, the definition of heat flux may differ from the classical thermal physics. In this work, we define the average heat flux in x direction as

$$q_x = \frac{1}{m \cdot n}\sum_{a=1}^{m}\sum_{b=1}^{n}\int_{4\pi} I(a,b)\cos\theta \mathrm{d}\Omega \tag{6}$$

where m and n are the number of grids used in calculations in x and y directions and they are chosen depending on various system sizes; therefore, the total grid number would be $m \cdot n$.

Although the systems' size is larger than the phonon MFP, many of them may ballistically transport. In order to keep the accuracy, we take the average temperature in $x = 0$ ($T_{\mathrm{avg}}(0)$) and $x = L$ ($T_{\mathrm{avg}}(L)$) to calculate the effective thermal conductivity.

$$T_{\mathrm{avg}}(0) = \frac{4\pi}{vc}\frac{1}{n}\sum_{b=1}^{n}\int_{4\pi} I(1,b)\cos\theta \mathrm{d}\Omega \tag{7}$$

$$T_{\mathrm{avg}}(L) = \frac{4\pi}{vc}\frac{1}{n}\sum_{b=1}^{n}\int_{4\pi} I(m,b)\cos\theta \mathrm{d}\Omega \tag{8}$$

The effective thermal conductivity would be

$$K_{\mathrm{eff.}} = \frac{\frac{1}{mn}\sum_{a=1}^{m}\sum_{b=1}^{n}\int_{4\pi} I(a,b)\cos\theta \mathrm{d}\Omega}{T_{\mathrm{avg}}(0) - T_{\mathrm{avg}}(L)} \tag{9}$$

3. Numerical method

Fig. 1a and b schematically illustrate the two kinds of porous nanostructures in which the pores are of in-line and staged arrangement, respectively. In both structures, when the system length in the z-direction is much larger than the phonon MFP, the effects of phonon transport of the two boundaries in the z-direction can be ignored, and the models can therefore be simplified to two-dimensional structures. Through Eq. (1), BTE can be presented as

$$\sin\theta\cos\phi\frac{\partial I}{\partial y} + \cos\theta\frac{\partial I}{\partial x} = \frac{\frac{1}{4\pi}\int_{4\pi} I\mathrm{d}\Omega - I_0}{\Lambda} \tag{10}$$

where θ and ϕ are polar and azimuthal angles; x and y are the coordinate directions as the definition in Fig. 1.

Previous studies of thermal radiation had generally used the discrete ordinate method (DOM, S_N method) to solve the radiative heat transfer equation. The DOM method assumes that the whole solid angle can be divided into N parts and that the phonon intensities in each part are equal. The average phonon intensity over the whole solid angle, $\int_{4\pi}(4\pi)^{-1} I\mathrm{d}\Omega$, can then be computed as follows [23]:

$$\frac{1}{4\pi}\int_{4\pi} I\mathrm{d}\Omega = \frac{1}{4\pi}\sum_{i=1}^{N} w_i I_i, \tag{11}$$

where w_i is the weight of the phonon transportation in direction i and satisfies $\sum_{i=1}^{N}(4\pi)^{-1}w_i = 1$. Substituting Eq. (11) into Eq. (10), the 2D BTE becomes a partial differential equation. The phonon intensity distribution in the present 2D porous nanostructure can then be simulated by solving Eq. (10) using finite-difference and S_N methods.

In the physical models shown in Fig. 1, it is assumed that the pores are absolutely adiabatic. We suppose that the vacuum pores insulate heat transfer. As phonons collide with these boundaries, they would be hampered and reflected. The boundaries of the pores are assumed as specular reflection, as shown in Fig. 1c. The boundary conditions of the pores are therefore given by

$$I(x,y,\theta,\phi) = I(x,y,-\theta,\phi)(\text{in the } x\text{-direction}), \tag{12}$$

and

$$I(x,y,\theta,\phi) = I(x,y,\theta,-\phi)(\text{in the } y\text{-direction}). \tag{13}$$

Adiabatic boundary conditions in the y-direction are assumed. The incident phonons are specularly reflected at the boundaries.

$$I(x,y,\theta,\phi) = I(x,y,\theta,-\phi). \tag{14}$$

As for x-directional boundaries, constant temperature boundary conditions are imposed, i.e. a relatively high temperature (T_{H}, 300 K) condition at the boundary located at $x = 0$ and a relatively low temperature (T_{L}, 299 K) condition at the boundary located at $x = L$. The temperature difference between these two boundaries is set to be 1 K.

In order to facilitate the observation on temperature, we define the parameter-dimensionless temperature. According to the definition of boundary at $x = 0$ ($T_{\mathrm{H}} = 300$ K) and $x = L$ ($T_{\mathrm{L}} = 299$ K), the temperature difference between two boundaries must be between 1 K and 0 K. The dimensionless temperature is defined as $\eta = (T - T_{\mathrm{avg.}}(L))/(T_{\mathrm{avg.}}(0) - T_{\mathrm{avg.}}(L))$; therefore, the dimensionless temperature distribution in this work would be between 1 K and 0 K, too. That is used to demonstrate the results of temperature distribution in this work.

It is vital to choose an optimum mesh size in numerical simulation and the number of grids depend on system size. We examine various sets of mesh size in each physical model. For example, as the system size is 1.0×10^4 μm in

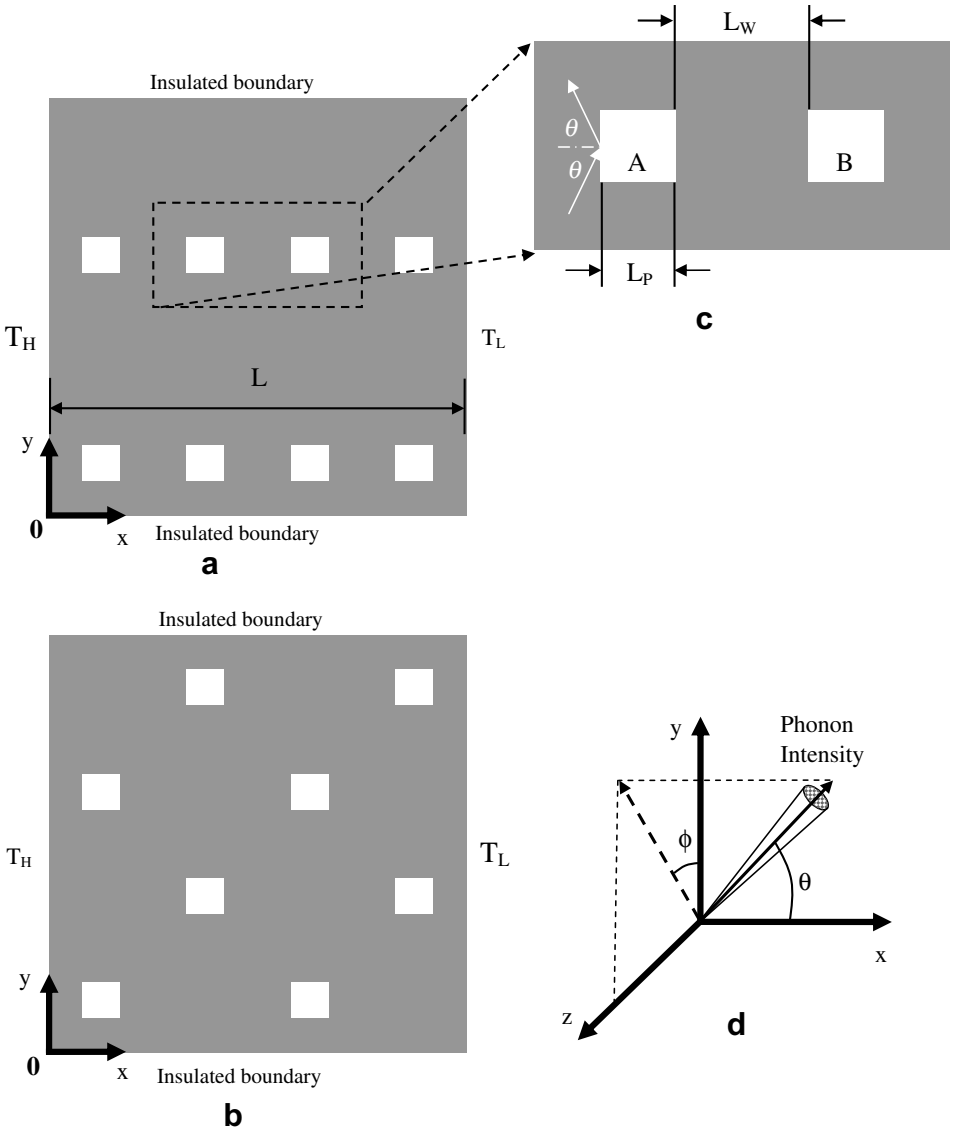

Fig. 1. Schematic diagrams of porous nanostructures: (a) pores arranged in aligned rows with specular reflection boundary condition; (b) pores arranged in staggered rows; (c) specular reflection boundary condition; and (d) phonon transport coordinate system.

single pore case, considering CPU time and accuracy, the ideal grid size would be 101×101. Furthermore, in order to verify the correctness, we minimize the pore size, and perceive that as the pore size shrinks, the thermal conductivity would become more and more close to the bulk value (as Fig. 2).

4. Results and discussion

This study simulates a unit cell model shown in Fig. 1c and the multi-pore models shown in Fig. 1a and b. Fig. 3a presents the dimensionless temperature distribution in a unit cell with a length of $L = 100$ nm and a pore size of $L_p = 20$ nm. It is clear that a high temperature area is formed near the left edge of the pore and a low temperature area formed near the right edge. As mentioned, the higher temperature boundary is located at $x = 0$. When the phonons collide with each other, some of them will be transported ballistically from $x = 0$ to $x = L$, while others will collide with the left pore boundary. These phonons are specularly reflected and transported ballistically back to $x = 0$. Previous studies [20] had indicated that in nanoscale structures, local thermal equilibrium may not be established, and the temperature in any particular region is related to the local energy density. This would explain the formation of the higher temperature region near the left boundary of the pore and the lower temperature region near the right boundary. Due to the scattering of high/low energy phonons at the boundaries of the pore, the high/low temperature areas (see Fig. 3b) represent the heat source and the heat sink, respectively, in the nanostructure. From Eq. (2), when ballistic transport domi-

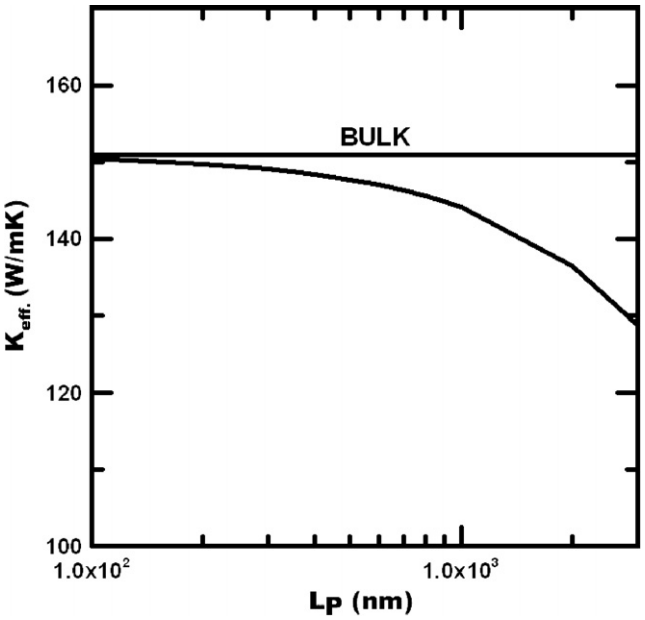

Fig. 2. Effects of pore size on the thermal conductivity of multi-pore nanostructure with structure size of $L = 10$ μm.

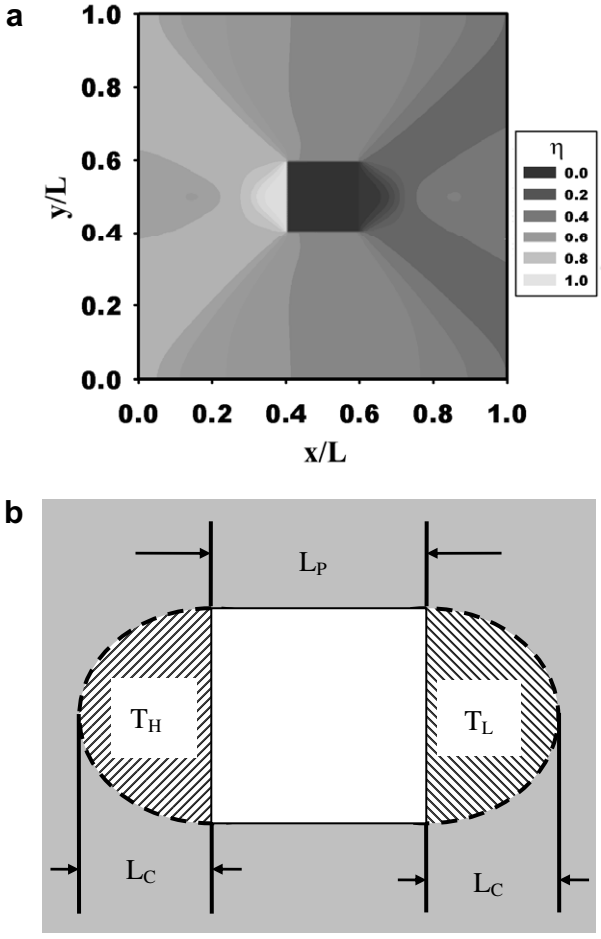

Fig. 3. (a) Dimensionless temperature contours of single pore nanostructure with structure size of $L = 100$ nm and pore size of $L_P = 20$ nm; and (b) regions affected by specular reflection boundary condition and ballistic phonon transport in single pore nanostructure.

nates, the term on the right hand side decreases with structure size (L). If L is much smaller than the MFP, Eq. (10) can be expressed as

$$\sin\theta\cos\phi\frac{\partial I}{\partial y} + \cos\theta\frac{\partial I}{\partial x} = 0. \tag{15}$$

In the high/low temperature areas, the temperature is almost uniform, and hence the variations of the phonon intensity in the x- and y-directions are almost the same. Solving Eq. (15) numerically indicates that the ratio of the high/low temperature region length, L_C, to the pore size, L_P, is found to be $L_C = 0.6475L_P$, as shown in Fig. 3b.

Fig. 4 shows the dimensionless temperature distributions of nanostructures with aligned-pore arrangement and a structure size of $L = 400$ nm. It is observed that the temperature distribution is dependent on the pore size. For the case of $L_p = 20$ nm, as shown in Fig. 4a, the phonons are scattered by the pore boundaries.

Fig. 5 refers to the correlation between effective thermal conductivity ($K_{eff.}$) and pore size. It is obvious that the effective thermal conductivity initially decreases with the pore size until $L_P = 45$ nm. At this pore size, the corresponding value of L_C calculated from Eq. (15) is approximately 27.5 nm. As a result, the high temperature (T_H) region may cover the low temperature (T_L) region. When the pore size is over 45 nm, the high-energy phonons from high temperature pore may merge with the low energy phonons from low temperature pore, which will decrease the effects of phonon scattering at the pore boundaries. In Fig. 4b, $L_P = 55$ nm, and the temperature in the T_H region is obviously lower than that of the corresponding region in Fig. 4a. In other words, as the pore size increases from 45 nm to 62 nm, larger pore size causes more merging of phonons, and results in a higher thermal conductivity, as shown in Fig. 5.

For a pore size of $L_P \approx 62$ nm, L_C is approximately 38 nm and the high-energy phonons scattered at high temperature pore collide with the boundaries of the low temperature pore and undergo secondary reflection. Fig. 4c shows that for a pore size of $L_P = 70$ nm, a second high temperature region is formed near the boundary of the low temperature pore as a of from secondary phonon scattering. Furthermore, it is seen that the phonon intensity becomes stronger as the pore size ranges from 62 nm to 75 nm. When L_P exceeds 75 nm, fewer phonons collide with the boundary and the scattered area decreases, as shown in Fig. 4d. However, as the pore size increases further, the temperature in the area between two neighboring pores becomes uniform as a result of the multi-reflection of phonons (see Fig. 4e).

Fig. 6 shows the variations of the thermal conductivity with different pore sizes in aligned structures. In the model with structure size being less than 2000 nm, ballistic phonon transport and independent scattering dominate the whole phonon transport process. For convenience, the following parameter of aspect ratio is defined to analyze the independent scattering effect on the thermal conductivity:

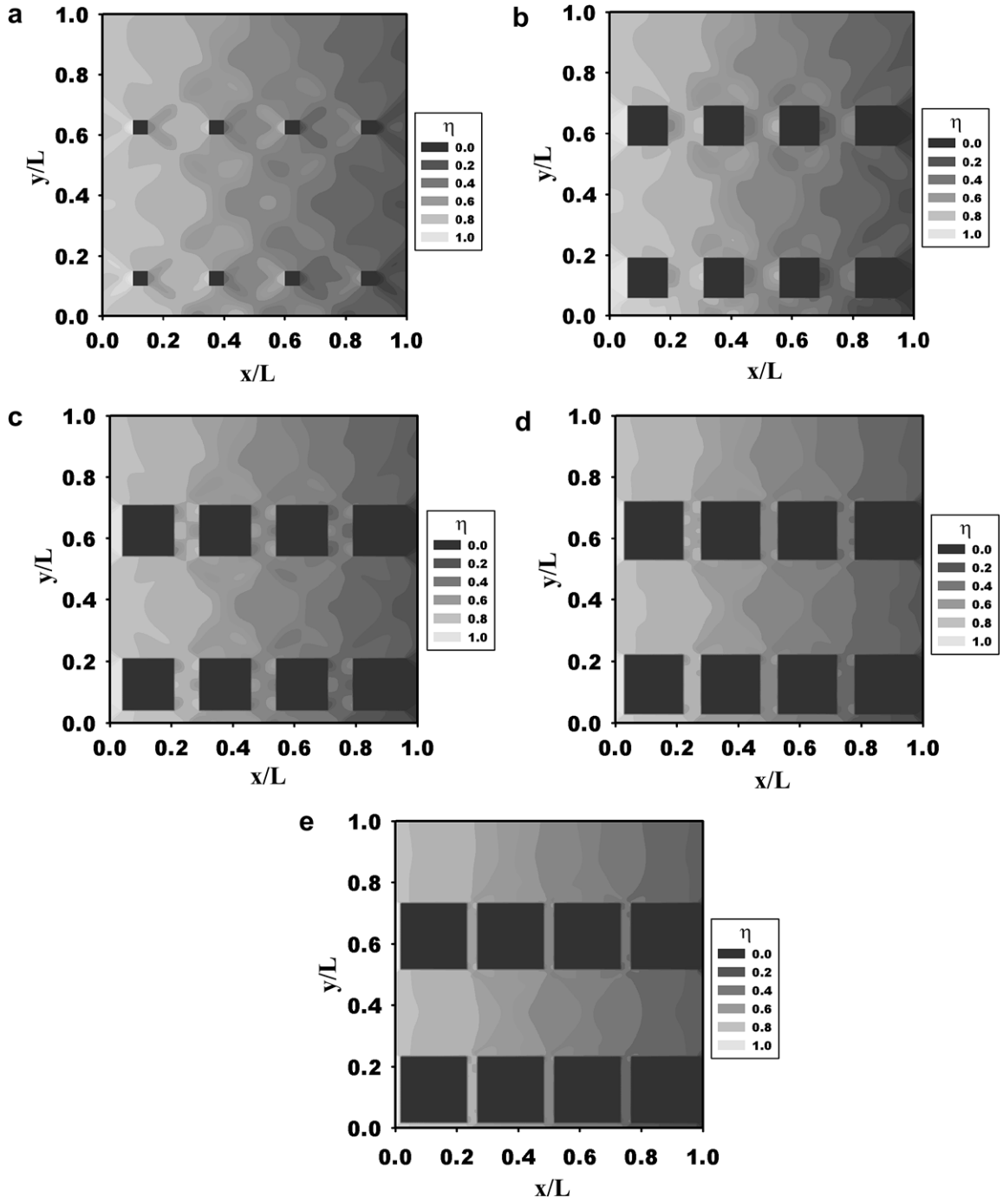

Fig. 4. Temperature contours of porous nanostructures with structure size of $L = 400$ nm in which the pores are arranged in aligned rows: (a) $L_P = 20$ nm; (b) $L_P = 55$ nm; (c) $L_P = 70$ nm; (d) $L_P = 80$ nm; and (e) $L_P = 90$ nm.

$$A = \frac{L_W}{L_P}, \tag{16}$$

where L_W is the spacing between two neighboring pores in the x-direction. Fig. 7 shows the variations of the thermal conductivity with the aspect ratio at different nanostructure size. When the value of the aspect ratio is less than 1.22, independent scattering dominates the phonon transport between two neighboring pores in the x-direction. The more effective the ballistic phonon transport, the more effective the independent scattering.

There are distinct differences between the aligned model and the staggered one. The most important phenomenon in the aligned structure is of dependent scattering. In the staggered model, L_W is much larger than L_C. Therefore, no matter how large the pores size is, dependent scattering does not occur. Fig. 8, in which the device size (L) and pores size are the same as the size in Fig. 4a–d, reveals that

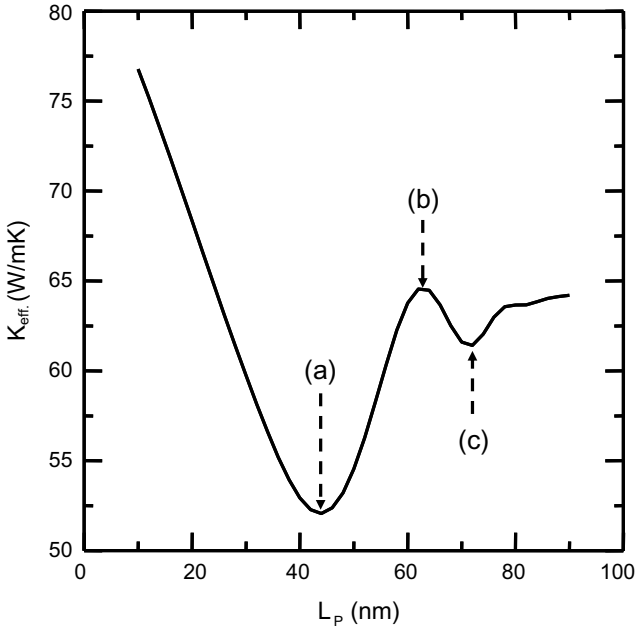

Fig. 5. Effects of pore size on the thermal conductivity of multi-pore nanostructure with structure size of $L = 400$ nm.

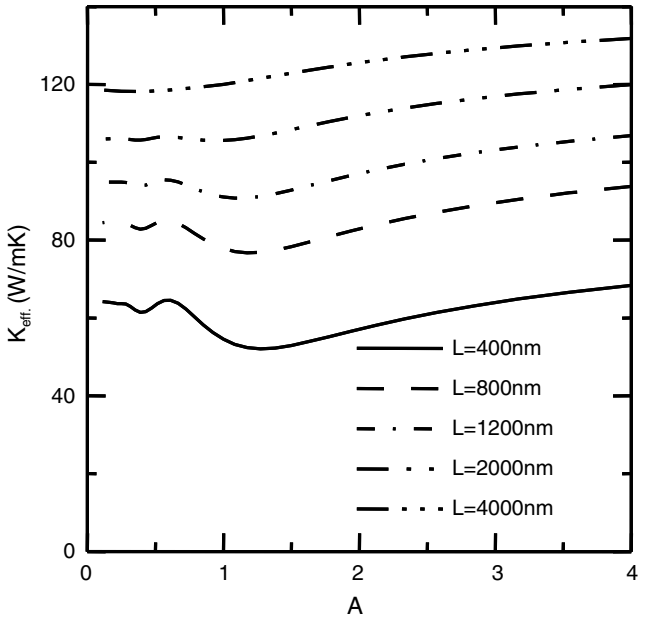

Fig. 7. Effects of pore aspect ratio on the thermal conductivity of multi-pore nanostructures as a function of structure size, L.

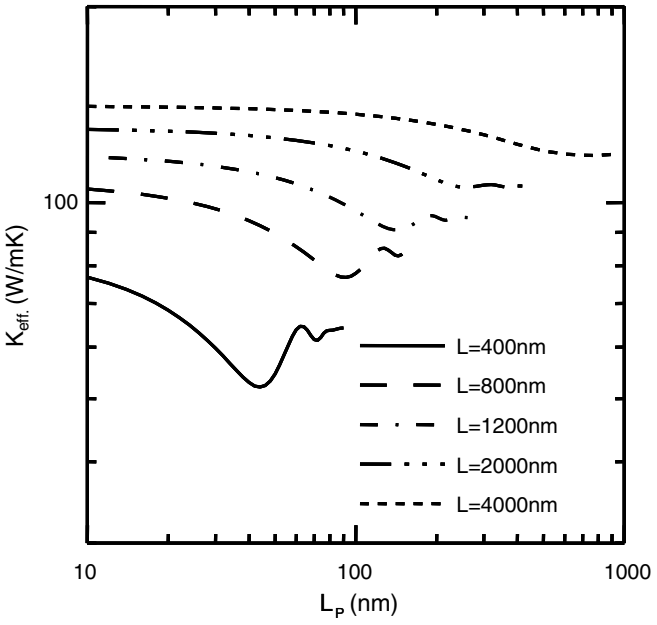

Fig. 6. Thermal conductivity of aligned porous nanostructure as a function of pore size.

as the pore size increases, L_C becomes larger in each pore. It means that more phonons are scattered, and the thermal conductivity becomes smaller. The results also can be found in Fig. 9; the thermal conductivity declines with increasing pore size. As the device size increases, size effect would be the minor mechanism and the thermal conductivity is close to the bulk value.

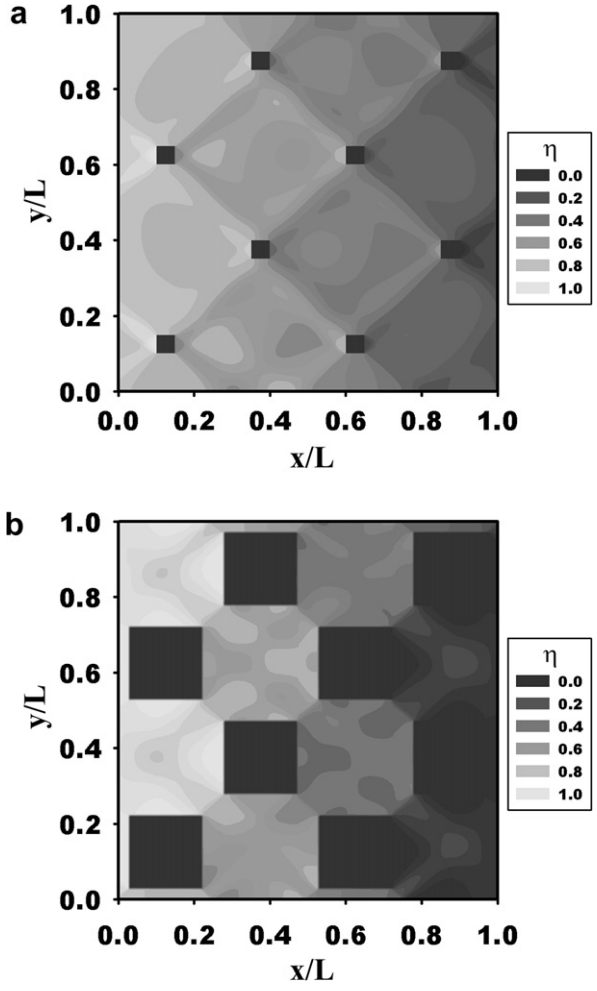

Fig. 8. Temperature contours in staggered porous nanostructure with $L = 400$ nm and pore size of: (a) $L_P = 20$ nm and (b) $L_P = 80$ nm.

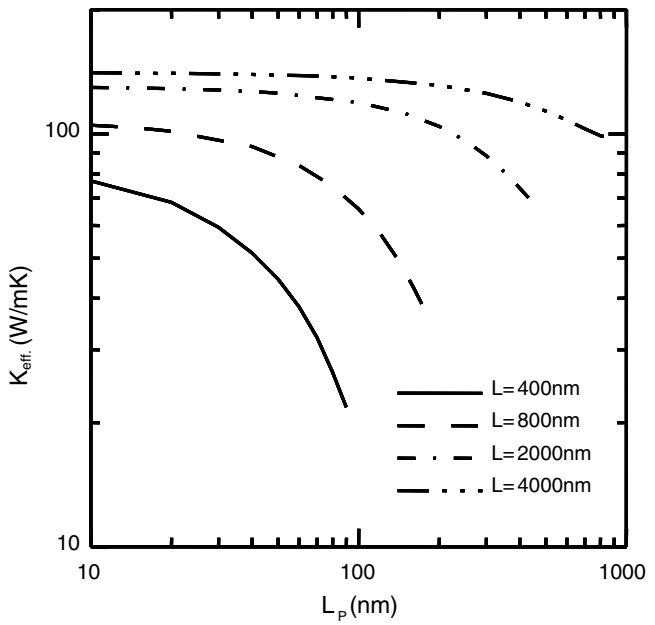

Fig. 9. Effects of pore size on the thermal conductivity of staggered porous nanostructure.

5. Conclusion

This study has numerically investigated the effects of the pore geometry and arrangement (i.e. aligned or staggered) on the thermal conductivity of a two-dimensional nanostructure. The following conclusions have been made.

1. The domination of ballistic phonon transport and specular reflection at the pore boundaries will cause serious impact on the heat transfer in porous nanostructure.
2. The pore boundaries in the heat flux direction block the passage of high-energy phonons and result in the formation of a high temperature region. When the aspect ratio exceeds 1.22, the thermal conductivity reduces with the aspect ratio in the aligned-pore.
3. The results show that the larger the pore size, the lower the thermal conductivity of the nanostructure.
4. It can be suggested that the staggered-pore nanostructures represent relatively smaller thermal conductivity than the staggered ones.

Acknowledgement

This study was supported by the National Science Council of the Republic of China, Taiwan, under Grant No. NSC 93-2212-E-211-011.

References

[1] D.M. Rowe, Thermoelectrics, Ph.D. Thesis, University of Wales, 1995.
[2] G. Mahan, B. Sales, J. Sharp, Thermoelectric materials: new approaches to an old problem, Phys. Today 50 (1997) 42–48.
[3] A. Majumdar, Thermoelectricity in semiconductor nanostructures, Science 303 (2004) 777–778.
[4] G. Chen, M. Neagu, Thermal conductivity and heat transfer in superlattices, Appl. Phys. Lett. 71 (1997) 2761–2763.
[5] G. Chen, Thermal conductivity and ballistic-phonon transport in the cross-plane direction of superlattice, Phys. Rev. B 57 (1998) 14958.
[6] Y. Zhang, G. Zeng, R. Singh, J. Christofferson, E. Croke, J.E. Bowers, A. Shakouri, Measurement of seebeck coefficient perpendicular to SiGe superlattice, in: Int. Conference on Thermoelectrics, Long Beach, CA, 2002.
[7] Y. SungtaekJu, Hung Ming-Tsung, Usui Takane, Nanoscale heat conduction across metal–dielectric interfaces, ASME J. Heat Transfer 128 (2006) 919–925.
[8] R. Venkatasubramanian, E. Siivola, T. Colpitts, B. O'Quinn, Thin-Film thermoelectric devices with high room-temperature figure of merit, Nature 413 (2001) 597–602.
[9] C.H. Huang, K.Y. Chen, An inverse phonon radiative transport problem in estimating the boundary temperatures for a double-layer nanoscale thin film, Numer. Heat Transfer, Part A 52 (2007) 43–70.
[10] A. Khitun, A. Balandin, J.L. Liu, K.L. Wang, In-plane lattice thermal conductivity of a quantum-dot superlattice, J. Appl. Phys. 88 (2000) 696–699.
[11] T.C. Harman, P.J. Taylor, M.P. Walsh, B.E. Laforge, Quantum dot superlattice thermoelectric materials and devices, Science 297 (2002) 2229–2232.
[12] J.L. Liu, A. Khitun, K.L. Wang, W.L. Liu, G. Chen, Q.H. Xie, S.G. Thomas, Cross-plane thermal conductivity of self-assembled Ge quantum dot superlattices, Phys. Rev. B 67 (2003) 165333.
[13] N. Mingo, Calculation of Si nanowire thermal conductivity using complete phonon dispersion relations, Phys. Rev. B 68 (2003) 113308.
[14] C. Dames, M.S. Dresselhaus, G. Chen, Phonon thermal conductivity of superlattice nanowires for thermoelectric applications, in: At MRS fall meeting of Thermoelectric Materials 2003 – Research and Applications, Boston, 2003.
[15] N. Mingo, Thermoelectric figure of merit and maximum power factor in III–V semiconductor nanowire, Appl. Phys. Lett. 84 (2004) 2652–2654.
[16] C. Dames, G. Chen, Theoretical phonon thermal conductivity of Si/Ge superlattice nanowires, J. Appl. Phys. 95 (2004) 682–693.
[17] Z.R. Zhong, X.W. Wang, J. Xu, Equilibrium molecular dynamics study of phonon thermal transport in nanomaterials, Numer. Heat Transfer, Part B 46 (2004) 429–446.
[18] W. Zhang, T.S. Fisher, N. Mingo, The atomistic Green's function method an efficient simulation approach for nanoscale phonon transport, Numer. Heat Transfer, Part B 51 (2007) 333–349.
[19] D. Song, G. Chen, Thermal conductivity of periodic microporous silicon films, Appl. Phys. Lett. 84 (2004) 687–689.
[20] R. Yang, G. Chen, Thermal conductivity modeling of periodic two-dimensional nanocomposites, Phys. Rev. B 69 (2004) 195316.
[21] Deyu Li, Scott T. Huxtable, Alexis R. Abramson, Arun Majumdar, Thermal transport in nanostructured solid-state cooling devices, ASME J. Heat Transfer 127 (2005) 108–114.
[22] C.L. Tien, G. Chen, Challenges in microscale conductive and radiative heat transfer, ASME J. Heat Transfer 116 (1994) 799–807.
[23] M.F. Modest, Radiative Heat Transfer, McGraw-Hill, New York, 1993.